ELSEVIER

Advances in Water Resources 24 (2001) 73–87

Advances in Water Resources

www.elsevier.com/locate/advwatres

The local discontinuous Galerkin method for contaminant transport

Vadym Aizinger [a,1], Clint Dawson [a,*,1], Bernardo Cockburn [b,2], Paul Castillo [b,2]

[a] *Center for Subsurface Modeling — C0200, Texas Institute for Computational and Applied Mathematics, University of Texas, Austin, TX 78712, USA*
[b] *School of Mathematics, University of Minnesota, Minneapolis, MN 55455, USA*

Received 15 November 1999; received in revised form 21 March 2000; accepted 24 March 2000

Abstract

We develop a discontinuous finite element method for advection–diffusion equations arising in contaminant transport problems, based on the Local Discontinuous Galerkin (LDG) method of Cockburn B and Shu CW. (The local discontinuous Garlerkin method for time-dependent convection–diffusion systems. SIAM J Numer Anal 1998;35:2440–63). This method is defined locally over each element, thus allowing for the use of different approximating polynomials in different elements. Furthermore, the elements do not have to conform, or "match-up" at interfaces. The method has a built-in upwinding mechanism for added stability. Moreover, it is conservative. We describe the method for multi-dimensional systems of equations with possibly non-linear adsorption terms, and provide some numerical results in both one and two dimensions. These results examine the accuracy of the method, and its ability to approximate solutions to some linear and non-linear problems arising in contaminant transport.

1. Introduction

The movement of contaminants through groundwater and surface water environments is modeled by transport equations, that is, equations which describe the advection, diffusion and interaction of contaminants within the environment. These equations are often advection-dominated, and thus require special care when solved numerically.

In recent years, there has been much interest in using *upwind* schemes for simulating such transport problems. These schemes are also referred to as *high resolution* or *shock-capturing* methods. An excellent survey of these types of methods in one-space-dimension is contained in [29]. They have been applied to contaminant transport in groundwater (see, for example, [1,22,24,26,27,32,37]) and in surface water (see, for example, [10,25,31,36,38]). In this paper, we will consider one particular type of shock-capturing scheme called the Discontinuous Galerkin method.

When using a high resolution method to approximate advection in an advection–diffusion equation, the question then is how to numerically incorporate the physical diffusion. When solving on structured grids, diffusion can easily be incorporated using central finite differences, as described in [22,23]. A more general approach, based on using the mixed finite element method for diffusion, has been proposed and analyzed in [9,18,23]. We refer to this approach as the upwind-mixed method. On structured grids, using special numerical integration rules, the upwind-mixed method reduces to a cell-centered finite difference method, as shown in [23]. In this paper, we will present a very different approach for incorporating diffusion based on an extension of the discontinuous Galerkin method, known as the Local Discontinuous Galerkin (LDG) method. Both the LDG and upwind-mixed methods have the favorable properties that they are based on conserving mass locally over each element and they approximate sharp fronts accurately and with minimal oscillation. Moreover, these methods are easily extendable to non-linear systems. The LDG method has some additional nice properties. In particular, it can easily be extended to higher order polynomials, defined on any grid including non-conforming grids, and easily allows one to vary the degree of the approximating space from one element to the next.

The application we will focus on is transport of one or more solutes through a homogeneous, saturated

* Corresponding author. Tel.: +1-512-475-8627; fax: +1-512-471-8694.
E-mail address: clint@ticam.utexas.edu (C. Dawson).

[1] Supported in part by National Science Foundation grants DMS-9873326 and DMS-9805491.
[2] Supported in part by National Science Foundation grant DMS-9807491 and the University of Minnesota Supercomputing Institute.

0309-1708/01/$ - see front matter
PII: S0309-1708(00)00022-1

porous medium. To show how the method can handle non-linearities, we will allow for non-linear adsorption kinetics. A particular problem of interest is competitive adsorption between species. We assume the flow to be at steady state, and the transport to be described by advection, molecular diffusion, mechanical dispersion and chemical reactions (adsorption) between a solute and the surrounding porous skeleton. Mathematically, this process is modeled by a possibly non-linear partial differential equation, in the case of contamination by one solute, or a non-linear coupled system of PDEs, if the fluid is contaminated by several substances.

Non-linear adsorption in porous media has recently been investigated by a number of authors, both mathematically and numerically. Van Duijn and Knabner [34] proved the existence of traveling wave solutions for models with equilibrium and non-equilibrium adsorption. Dawson et al. and Barrett and Knabner developed Galerkin and characteristic-Galerkin methods for models with non-equilibrium adsorption, and analyzed them in [3,4,21]. Recently, the second author in collaboration with van Duijn and Grundy applied the upwind-mixed method mentioned above to the study of equilibrium adsorption. In [20,28,33], the long-time behavior of these equations was investigated both mathematically and numerically. The upwind-mixed method used in these papers was analyzed in [22]. All of this work has been for a single-component: the literature is sparser for multi-component models. Rhee et al. [30] studied the characteristic structure of one-dimensional, multi-component models, and provided some analytical solutions for certain initial and boundary conditions.

The paper is divided into the following sections: In Section 2, we present the mathematical model of transport we will consider, including non-linear adsorption. In Section 3, we describe the LDG method, present some of the theory behind the method and give some numerical results illustrating the convergence of the method on smooth test problems. In Section 4, we discuss implementation details of the methods, including time-stepping and stability post-processing needed to suppress oscillations. In Section 5, we present results for both methods applied to transport problems with non-linear adsorption. Section 6 concludes the paper with a brief discussion of the numerical results.

2. Mathematical model of contaminant transport in porous medium

For one component, mass conservation of the contaminant gives the equation [30]

$$\phi c_t + (1-\phi)\tilde{s}_t + \nabla \cdot (uc - D\nabla c) = f(c), \tag{1}$$

where c is the concentration of solute in moles per unit volume in the fluid phase, $\tilde{s}(x,t)$ the concentration of contaminant adsorbed on the solid matrix in moles per unit volume of solid, $\phi > 0$ the porosity, u the Darcy velocity, D the molecular diffusion and mechanical dispersion, and f models source/sink terms which could be dependent on concentration.

The chemical reactions describing adsorption may be fast (equilibrium) or slow (non-equilibrium) depending on the rate of reaction with respect to the rate of flow. In the case of equilibrium adsorption reactions, the contaminant adsorbed by the solid is generally assumed to be a function of the concentration in the fluid; that is,

$$\tilde{s} = a(c). \tag{2}$$

In the case of non-equilibrium adsorption reactions, $\tilde{s}$ is generally assumed to satisfy

$$\tilde{s}_t = k(a(c) - \tilde{s}), \tag{3}$$

where k is a rate parameter. Thus, (2) is obtained in the limit as $k \to \infty$. Here, we will concentrate only on the equilibrium case. The function a in (2) and (3) is called an adsorption isotherm. Common isotherms are the Langmuir isotherm

$$a(c) = \frac{NKc}{1+Kc}, \qquad K > 0, \tag{4}$$

where N is the saturation concentration of the adsorbed solute, and the Freundlich isotherm

$$a(c) = Kc^p, \quad K > 0, \tag{5}$$

see [35]. In (5), $p \in (0,1]$ is commonly chosen.

In this paper, we consider the case of equilibrium adsorption. Substituting (2) into (1), letting

$$A(c) = (1-\phi)a(c), \tag{6}$$

we obtain

$$\phi c_t + A(c)_t + \nabla \cdot (uc - D\nabla c) = f. \tag{7}$$

We solve (7) on a domain $\Omega \subset \mathbb{R}^d$ for $t > 0$. Letting ν denote the unit outward normal to $\Gamma \equiv \partial\Omega$, we impose "inflow" and "outflow" boundary conditions

$$(uc - D\nabla c) \cdot \nu = uc_{\mathrm{I}}(t) \cdot \nu, \quad t > 0, \tag{8}$$

$$(D\nabla c) \cdot \nu = 0, \quad t > 0. \tag{9}$$

Here $c_{\mathrm{I}}(t)$ is a specified inflow concentration. The inflow condition (8) is imposed, where $u \cdot \nu < 0$, and the outflow condition (9) is imposed otherwise. We denote the inflow portion of the boundary by Γ_{I} and the outflow/noflow part by Γ_{O}.

We also assume the initial condition

$$c(x,0) = c^0(x), \quad x \in \Omega. \tag{10}$$

We note that A is a strictly monotone increasing function of c in both the Langmuir and Freundlich isotherms: therefore, (7) is uniformly parabolic if $c > 0$. If $a(c)$ is of Freundlich type, however, then (7) is degenerate parabolic for $p < 1$ and $c \geqslant 0$, since $a'(c)$ blows-up as $c \downarrow 0$.

We are also interested in the case of multi-component contaminant transport with competitive adsorption between species. In this case, we assume a similar equation in each component holds

$$\phi \mathbf{c}_t + \mathbf{A}(\mathbf{c})_t + \nabla \cdot (u\mathbf{c} - D\nabla \mathbf{c}) = \mathbf{f}, \quad x \in \Omega, \ t > 0, \tag{11}$$

$$\mathbf{A}(\mathbf{c}) = (1-\phi)\,\mathbf{a}(\mathbf{c}), \tag{12}$$

where $\mathbf{c} = (c_1, c_2, \ldots, c_n)^{\mathrm{T}}$ and n is the number of components.

The Langmuir isotherm in the multi-component case is [30]

$$\mathbf{a}(\mathbf{c}) = (a_1(\mathbf{c}), a_2(\mathbf{c}), \ldots, a_n(\mathbf{c}))^{\mathrm{T}}, \tag{13}$$

where

$$a_i(\mathbf{c}) = \frac{N_i K_i c_i}{1 + K_1 c_1 + K_2 c_2 + \cdots + K_n c_n}, \quad K_i > 0, \quad i = 1, \ldots, n. \tag{14}$$

Here N_i stands for the maximum number of moles of solute i that can be adsorbed per unit volume of adsorbent.

We augment (11) with the initial and boundary conditions

$$\mathbf{c}(x,0) = \mathbf{c}^0(x), \quad x \in \Omega, \tag{15}$$

$$(u\mathbf{c} - D\nabla \mathbf{c}) \cdot v = u\mathbf{c}_{\mathrm{I}}(t) \cdot v, \ \Gamma_{\mathrm{I}} \times (0,T], \tag{16}$$

$$(D\nabla \mathbf{c}) \cdot v = 0, \ \Gamma_{\mathrm{O}} \times (0,T]. \tag{17}$$

3. The LDG method

The LDG method [16] was developed as a modification for non-linear parabolic problems of the so-called Runge–Kutta Discontinuous Galerkin (RKDG) method designed originally for non-linear hyperbolic problems of the form

$$c_t + \nabla \cdot g(c) = 0.$$

The main idea of the LDG method is to suitably rewrite the parabolic problem under consideration into a larger degenerate first-order system and then discretize it using the RKDG method. Similar to the RKDG method, the resulting scheme is a highly parallelizable method of potentially high-order accuracy.

3.1. Formulation of the method

We will describe the LDG method for the scalar equation (7). The extension to the system (11) is straightforward. We first introduce two new variables

$$\tilde{z} = -\nabla c,$$

and

$$z = D\tilde{z}.$$

We also define

$$s(x,t) = \phi c(x,t) + A(c(x,t)) \tag{18}$$

and rewrite the problem (7) as follows:

$$s_t + \nabla \cdot (uc + z) = f, \tag{19}$$

$$\tilde{z} + \nabla c = 0, \tag{20}$$

$$z = D\tilde{z}. \tag{21}$$

Before describing the LDG method for (19)–(21) we define some notation. On any spatial domain R let $(\cdot,\cdot)_R$ denote the $L^2(R)$ inner product, where we omit R if $R = \Omega$. To distinguish integration over domains $R \in \mathbb{R}^{d-1}$ (e.g., surfaces or lines), we will use the notation $\langle \cdot,\cdot \rangle_R$. Let $\{\mathscr{T}_h\}_{h>0}$ denote a family of finite element partitions of Ω such that no element Ω_e crosses the boundaries of Γ_{I} or Γ_{O}, where h is the maximal element diameter. Let

$$W_{h,e} = \{w : w \text{ is a polynomial of degree } \leqslant k_e \text{ on each element } \Omega_e \text{ in } \mathscr{T}_h\}. \tag{22}$$

Note that the degree k_e could vary from one element to the next. Let n_e denote the unit outward normal to $\partial\Omega_e$. Then, for $x \in \partial\Omega_e$ we define

$$w^-(x) = \lim_{s \to 0^-} w(x + sn_e),$$

and

$$w^+(x) = \lim_{s \to 0^+} w(x + sn_e).$$

That is, w^- is the value of w to the "left" of the boundary, assuming the normal n_e points from "left" to "right." We also define

$$\overline{w} = (w^+ + w^-)/2. \tag{23}$$

We seek approximations $C, Z, \tilde{Z}$ to $c, z, \tilde{z}$, where on Ω_e, $C \in W_{h,e}$ and $Z, \tilde{Z} \in (W_{h,e})^d$. We first note that, multiplying (19)–(21) by arbitrary test functions $w \in H^1(\Omega_e)$, $v, \tilde{v} \in (H^1(\Omega_e))^d$, respectively, and integrating over any element Ω_e, we get, after integration by parts

$$(s_t, w)_{\Omega_e} - (uc + z, \nabla w)_{\Omega_e} + \langle (uc+z) \cdot n_e, w^- \rangle_{\partial\Omega_e} = (f, w)_{\Omega_e}, \tag{24}$$

$$(\tilde{z}, v)_{\Omega_e} - (c, \nabla \cdot v)_{\Omega_e} + \langle c, v^- \cdot n_e \rangle_{\partial\Omega_e} = 0, \tag{25}$$

$$(z, \tilde{v})_{\Omega_e} = (D\tilde{z}, \tilde{v})_{\Omega_e}. \tag{26}$$

Next, we replace c, z, and $\tilde{z}$ by approximations C, Z, and $\tilde{Z}$, respectively, and restrict our test functions to lie in the approximating space. Since C, Z and $\tilde{Z}$ are allowed to be discontinuous across element boundaries, we must also define how the boundary integrals are approximated. These are computed by upwinding C in the advection term, and averaging C and Z in the other boundary integrals. Define the upwind value C^u on an element boundary as follows:

$$C^u = \begin{cases} C^- & \text{if } u \cdot n_e \geqslant 0, \\ C^+ & \text{if } u \cdot n_e < 0. \end{cases} \tag{27}$$

Then, the approximate solution given by the LDG method is defined as the solution of the following weak formulation:

$$(S_t, w)_{\Omega_e} - (uC + Z, \nabla w)_{\Omega_e} + \langle C^u u \cdot n_e, w^- \rangle_{\partial\Omega_e} + \langle \overline{Z} \cdot n_e, w^- \rangle_{\partial\Omega_e} = (f, w)_{\Omega_e}, \quad w \in W_{h_e}, \tag{28}$$

$$(\tilde{Z}, v)_{\Omega_e} - (C, \nabla \cdot v)_{\Omega_e} + \langle \overline{C}, v^- \cdot n_e \rangle_{\partial\Omega_e} = 0, \quad v \in (W_{h_e})^d, \tag{29}$$

and

$$(Z, \tilde{v})_{\Omega_e} = (D\tilde{Z}, \tilde{v})_{\Omega_e}, \quad \tilde{v} \in (W_{h_e})^d. \tag{30}$$

Here $S = \phi C + A(C)$.

The initial condition is enforced by

$$(C(\cdot, 0), v_h)_{\Omega_e} = (c^0(\cdot), v_h)_{\Omega_e}. \tag{31}$$

The boundary conditions are enforced by modifying the above equations as follows. On the inflow boundary Γ_I, we set

$$\langle C^u u \cdot n_e, w^- \rangle_{\partial\Omega_e \cap \Gamma_I} + \langle \overline{Z} \cdot n_e, w^- \rangle_{\partial\Omega_e \cap \Gamma_I} = \langle c_I u \cdot n_e, w^- \rangle_{\partial\Omega_e \cap \Gamma_I}, \tag{32}$$

in (28). On Γ_O, we set

$$\langle \overline{Z} \cdot n_e, w^- \rangle_{\partial\Omega_e \cap \Gamma_O} = 0 \tag{33}$$

in (28) and replace $\overline{C}$ by C^- in (29).

Remark 1. The solution $\tilde{Z}$ can be resolved element by element in terms of C by using (29). Furthermore, Z can be expressed in terms of $\tilde{Z}$ on each element using (30). Substituting these relations into (28), one ends up solving for C unknowns only.

Remark 2. The element Ω_e can be very general. Theoretically, the only requirement is that it has a Lipschitz boundary [5]. Furthermore, elements and their neighbors do not have to match-up along the edges. Therefore, one can locally refine elements without worrying about hanging nodes. Also, as noted above, the degree of polynomial used to define C can vary from one element to the next without any difficulty.

Remark 3. The method (28)–(30) is conservative in the following sense. Letting $w = 1$ on Ω_e and zero elsewhere, we find

$$(S_t, 1)_{\Omega_e} + \langle C^u u \cdot n_e, 1 \rangle_{\partial\Omega_e} + \langle \overline{Z} \cdot n_e, 1 \rangle_{\partial\Omega_e} = (f, 1)_{\Omega_e}. \tag{34}$$

The true solution satisfies

$$(s_t, 1)_{\Omega_e} + \langle cu \cdot n_e, 1 \rangle_{\partial\Omega_e} + \langle z \cdot n_e, 1 \rangle_{\partial\Omega_e} = (f, 1)_{\Omega_e}, \tag{35}$$

which is a statement of local conservation of mass. Summing over all elements, and integrating in time from 0 to T, we find

$$\int_\Omega S(\cdot, T)\, d\Omega = \int_\Omega S(\cdot, 0)\, d\Omega + \int_0^T \int_\Omega f\, d\Omega\, dt - \int_0^T \int_{\Gamma_I} c_I u \cdot v\, ds\, dt - \int_0^T \int_{\Gamma_O} C^- u \cdot v\, ds\, dt, \tag{36}$$

which is a statement of global conservation and is also satisfied by the true solution.

Remark 4. While the boundary conditions (8) and (9) may be the most natural to use in applications, for the purpose of testing the algorithm we have implemented primarily Dirichlet boundary conditions. A Dirichlet condition

$$c = \tilde{c} \tag{37}$$

on $\partial\Omega$ can be enforced by setting $\overline{Z} = Z^-$ in (28) and $\overline{C} = \tilde{c}$ in (29) when integrating over the boundary. Moreover, in the definition of C^u in (27) we set $C^+ = \tilde{c}$ on $\partial\Omega$.

To illustrate the method for a simple problem, consider the equation

$$c_t + c_x - c_{xx} = f, \tag{38}$$

on the unit interval $[0, 1]$ with the boundary conditions

$$c - c_x = c_I, \quad x = 0, \tag{39}$$

$$c_x = 0, \quad x = 1. \tag{40}$$

In this case, $\tilde{z} = z = -c_x$. Let $0 = x_{1/2} < x_{3/2} < \cdots < x_{N+1/2} = 1$ denote a partition of the interval into subintervals B_j with midpoint $x_j = (x_{j-1/2} + x_{j+1/2})/2$ and length Δx. Consider the LDG method with $k_e = 0$, that is, piecewise constant approximations. Let C_j, Z_j denote these constant approximations on subinterval B_j. Then from (29) we find

$$Z_j = -\frac{\overline{C}(x_{j+1/2}) - \overline{C}(x_{j-1/2})}{\Delta x} = -\frac{C_{j+1} - C_{j-1}}{2\Delta x}. \tag{41}$$

From (28), we find for interior subintervals,

$$(C_j)_t + \frac{C_j - C_{j-1}}{\Delta x} + \frac{\overline{Z}(x_{j+1/2}) - \overline{Z}(x_{j-1/2})}{\Delta x} = \int_{B_j} f\, dx. \tag{42}$$

For $j = 1$, we have

$$(C_j)_t + \frac{C_j - c_I}{\Delta x} + \frac{\overline{Z}(x_{j+1/2})}{\Delta x} = \int_{B_j} f\, dx,$$

and for $j = N$,

$$(C_j)_t + \frac{C_j - C_{j-1}}{\Delta x} - \frac{\overline{Z}(x_{j-1/2})}{\Delta x} = \int_{B_j} f \, dx,$$

where $\overline{Z}(x_{j+1/2}) = (Z_j + Z_{j+1})/2$.

Substituting (41) into (42) we find that away from the boundaries,

$$(C_j)_t + \frac{C_j - C_{j-1}}{\Delta x} - \frac{C_{j+2} - 2C_j + C_{j-2}}{2\Delta x^2} = \int_{B_j} f \, dx. \quad (43)$$

This equation reveals a fairly wide stencil for the method. In [16], a slight modification to the LDG method is discussed, which reduces the stencil to only involve C_j, C_{j-1}, C_{j+1}. However, in general, for the LDG method the unknowns in any element Ω_e depend on the neighbors of Ω_e (elements which share all or part of an edge, excluding vertices), and the neighbors of the neighbors.

At this point, we have not discussed the time discretization for the method. We postpone this discussion to Section 4.

3.2. Stability results and error estimates

In this subsection, we state briefly some theoretical results for the method above. These estimates are for equations without the time derivative term $A(c)_t$ in (7) and for a single scalar equation. Extension of these estimates to the non-linear systems considered in this paper is the subject of future work. However, the estimates stated here give some insight into the performance of the method.

The LDG method was first analyzed by Cockburn and Shu [16]. They proved stability for the non-linear parabolic equation

$$c_t + f(c)_x - (d(c)c_x)_x = 0, \quad 0 < x < L, \quad t > 0, \quad (44)$$

and its multi-dimensional extension, under the assumption of periodic boundary conditions on c, and assuming f and d are Lipschitz.

Theorem 3.1 ($\mathbf{L}^2$-stability). *We have*

$$\frac{1}{2}\int_0^L C^2(x,T)\,dx + \int_0^T \int_0^L Z^2(x,t)\,dx\,dt \leqslant \frac{1}{2}\int_0^L (c^0)^2(x)\,dx. \quad (45)$$

We denote the $\mathbf{L}^2(0,L)$-norm of the ℓth derivative of c by $|c|_\ell$. In the linear case, $f'(\cdot) \equiv p$ and $d(\cdot) \equiv d$, from the above stability result and from the approximation properties of the finite element space W_h, Cockburn and Shu proved the following error estimate:

Theorem 3.2 ($\mathbf{L}^2$-error estimate). *Let* $\mathbf{e}$ *be the approximation error* $\mathbf{e} = \mathbf{w} - \mathbf{w}_h$. *Then we have,*

$$\left\{ \int_0^L |(c-C)(x,T)|^2\,dx + \int_0^T \int_0^L |(z-Z)(x,t)|^2\,dx\,dt \right\}^{1/2} \leqslant K\Delta x^k, \quad (46)$$

where $K = K(k, |c|_{k+1}, |c|_{k+2})$. *In the purely hyperbolic case* $d = 0$, *the constant* K *is of an order* $\Delta x^{1/2}$ *and in the purely parabolic case* $p = 0$, *the constant* K *is of an order* Δx *for even values of* k *for uniform grids.*

This result is somewhat pessimistic, in particular, for $k = 0$ it does not give any convergence rate when $d > 0$, $p \neq 0$ and the mesh is non-uniform. However, Castillo et al. [8] have recently derived an improved result in one-space-dimension for constant coefficients, which indicates that the method converges with rate Δx^{k+1}, as we have observed numerically below.

For general linear multi-dimensional advection–diffusion problems, the best rate of convergence that can be proved for the method is order k. For example, for the problem given by (7) with boundary conditions (8) and (9), Cockburn and Dawson have recently derived the following stability and error estimates [11]. As noted above, these results assume $A(c) = 0$ but would also extend to the case where A is linear in c.

Theorem 3.3 (Stability). *The scheme* (28)–(30) *satisfies*

$$\sum_e \left[\frac{1}{4} \max_{[0,T]} ||\phi^{1/2} C||^2_{\Omega_e} + \int_0^T (D\tilde{Z}, \tilde{Z})_{\Omega_e}\,dt \right] \leqslant \frac{1}{2}||\phi^{1/2}c^0||^2 + \sum_e \left\{ \int_0^T ||\phi^{1/2} f||_{\Omega_e}\,dt \right\}^2 + \frac{1}{2}\int_0^T ||c_1|u\cdot n|^{1/2}||^2_{\Gamma_1}\,dt. \quad (47)$$

In particular, the scheme satisfies (47) *for* $D \geqslant 0$. *If* $f = 0$, *then the* 1/4 *on the left-hand side of* (47) *is replaced by* 1/2.

Theorem 3.4 (Error estimate). *The scheme* (28)–(30) *satisfies*

$$\left\{ \sum_e \left[\frac{1}{4} \max_{[0,T]} ||\phi^{1/2}(C-c)||^2_{\Omega_e} + \int_0^T (D(\tilde{Z}-\tilde{z}), (\tilde{Z}-\tilde{z}))_{\Omega_e}\,dt \right] \right\}^{1/2} \leqslant Kh^k,$$

for c *sufficiently smooth, where* $k = \min_e k_e$.

An improved estimate of order $k + 1/2$ or $k + 1$ for the error $C - c$ in the norm

$$\left\{ \int_0^T ||C-c||^2_{L^2(\Omega)}\,dt \right\}^{1/2}$$

can be obtained by adding "penalty" terms to the method. These penalty terms penalize the jumps in the solution across interelement boundaries. A complete discussion of penalties along with the error estimates can be found in [7,19].

3.3. Implementation and numerical results

In this subsection, we present test runs on some smooth problems with known true solutions to obtain experimental rates of convergence. The results of numerical experiments demonstrating the performance of the LDG method on some contaminant transport problems will be presented in Section 5.

Above we formulated a semi-discrete LDG scheme, which requires some procedure to be used for time-stepping. Some Runge–Kutta schemes suitable for this purpose will be discussed in Section 4. In the following numerical examples, the order of the employed time-stepping scheme was high enough so that the error of the time-stepping procedure was negligible compared to the error of the LDG method.

Note that all time-stepping schemes used for examples in this section are of explicit type, therefore there is a restriction on the ratio between the length of the time step and the element size in the space domain. In most of these examples, the time steps are chosen sufficiently small so that temporal errors are almost negligible.

First, we provide the results of some numerical experiments for the following scalar equation with constant coefficients $u > 0$, $D \geqslant 0$:

$$\begin{aligned} L(c) &= c_t + A(c)_t + uc_x - Dc_{xx} \\ &= L(\sin 2\pi(x-t)+2), \quad 0 < x < 1, \ t > 0, \end{aligned} \tag{48}$$

with the initial and Dirichlet boundary conditions

$$c(x,0) = \sin 2\pi x + 2, \quad 0 < x < 1, \tag{49}$$

$$c(0,t) = -\sin 2\pi t + 2, \quad t > 0, \tag{50}$$

$$c(1,t) = -\sin(2\pi(1-t)) + 2, \quad t > 0, \tag{51}$$

where the right-hand side is obtained by plugging the function

$$c(x,t) = \sin 2\pi(x-t) + 2 \tag{52}$$

into Eq. (7). Eq. (52) is obviously the exact solution of (48)–(50). Here, the isotherm has the form

$$A(c) = \frac{c}{1+c}. \tag{53}$$

We compute our numerical solution up to $T = 0.5$ using the LDG method with approximating spaces of uniform degree k, $k = 0, 1, 2$. Elements with equal size are used. Time discretization is by a third-order accurate Runge–Kutta method. We list the $L^\infty(0,T;L^2)$ and $L^2(0,T;L^2)$ norms of the error for the functions $s = \phi c + A(c)$ and z, respectively.

The results of the numerical experiment in Table 1 show that, though for even degrees of approximating polynomials we retrieve the optimal order of convergence of Δx^{k+1}, for $k = 1$ we lose one power of Δx in the convergence rate of the flux. This can be improved if one modifies the scheme slightly as described in [8].

In Table 2, we consider the purely hyperbolic advection equation obtained from (48) by setting $D = 0$. In this case, we obtain experimental orders of convergence around Δx^{k+1} for all $k = 0, 1, 2$.

We performed similar tests for the coupled system consisting of two equations

$$\begin{aligned} \mathbf{L}(\mathbf{c}) &= \mathbf{c}_t + \mathbf{A}(\mathbf{c})_t + u\mathbf{c}_x - D\mathbf{c}_{xx} \\ &= \mathbf{L}\begin{pmatrix} \sin 2\pi(x-t)+2 \\ \cos 2\pi(x-t)+2 \end{pmatrix}, \quad 0 < x < 1, \ t > 0, \end{aligned} \tag{54}$$

Table 1
Advection-dominated advection–diffusion equation $u = 1$, $D = 0.01$

k	Var.	Norm	$N = 40$	$N = 80$		$N = 160$	
			Error	Error	Order	Error	Order
0	s	$L^\infty(0,T;L^2)$	1.21e − 01	6.32e − 02	0.94	3.23e − 02	0.97
	z	$L^2(0,T;L^2)$	4.76e − 02	2.64e − 02	0.85	1.39e − 02	0.93
1	s	$L^\infty(0,T;L^2)$	1.27e − 03	3.26e − 04	1.96	8.52e − 05	1.94
	z	$L^2(0,T;L^2)$	1.35e − 02	6.95e − 03	0.96	3.51e − 03	0.99
2	s	$L^\infty(0,T;L^2)$	1.06e − 05	1.25e − 06	3.08	1.54e − 07	3.02
	z	$L^2(0,T;L^2)$	6.48e − 05	8.41e − 06	2.95	1.09e − 06	2.95

Table 2
Advection (purely hyperbolic) equation $u = 1$, $D = 0$

k	Var.	Norm	$N = 40$	$N = 80$		$N = 160$	
			Error	Error	Order	Error	Order
0	s	$L^\infty(0,T;L^2)$	1.37e − 01	7.30e − 02	0.91	3.78e − 02	0.95
1	s	$L^\infty(0,T;L^2)$	1.21e − 03	3.02e − 04	2.00	7.56e − 05	2.00
2	s	$L^\infty(0,T;L^2)$	1.94e − 05	2.11e − 06	3.20	2.38e − 07	3.15

with the initial and boundary conditions

$$\mathbf{c}(x,0) = \begin{pmatrix} \sin 2\pi x + 2 \\ \cos 2\pi x + 2 \end{pmatrix} \quad \text{on } (0,1), \tag{55}$$

$$\mathbf{c}(0,t) = \begin{pmatrix} -\sin 2\pi t + 2 \\ \cos 2\pi t + 2 \end{pmatrix} \quad \text{for } t > 0, \tag{56}$$

$$\mathbf{c}(1,t) = \begin{pmatrix} -\sin 2\pi(1-t) + 2 \\ \cos 2\pi(1-t) \end{pmatrix} \quad \text{for } t > 0. \tag{57}$$

The Langmuir isotherm in its two-component form is

$$\mathbf{A}(\mathbf{c}) = \begin{pmatrix} \frac{R_1 K_1 c_1}{1+K_1 c_1+K_2 c_2} \\ \frac{R_2 K_2 c_2}{1+K_1 c_1+K_2 c_2} \end{pmatrix}, \tag{58}$$

and we have chosen $R_1 = R_2 = K_1 = 1$, $K_2 = 10$. The right-hand side vector-function is obtained by plugging the vector-function

$$\mathbf{c}(x,t) = \begin{pmatrix} \sin 2\pi(x-t) + 2 \\ \cos 2\pi(x-t) + 2 \end{pmatrix} \tag{59}$$

into (54). Numerical rates of convergence for this case are given in Table 3.

Similar to the scalar case, we observe here the experimental order of convergence of about Δx^{k+1} for the even degrees of approximating polynomials and some suboptimal order of convergence for the diffusive flux z for the odd degrees.

Finally, we computed an approximate solution to the purely hyperbolic system, obtained from (54) by setting $D = 0$. Here again, the experimental orders of convergence are of the order Δx^{k+1} for all $k = 0, 1, 2$. These results are given in Table 4.

4. Time-stepping schemes and stability post-processing

We can rewrite formally the semi-discrete problem (28) for the LDG method as

$$\mathbf{y}'(t) = \mathbf{L}_h(\mathbf{y}(t), t). \tag{60}$$

Traditional Runge–Kutta schemes as described in [6] applied to problems with discontinuous or very rough true solutions may lead to oscillatory approximate solutions. In order to reduce oscillations but retain a higher order of approximation, a new class of Runge–Kutta methods called RKΛΠP has been developed for these problems, see ([12–15,17]).

The main idea behind the RKΛΠP method is, first, to reformulate the explicit Runge–Kutta scheme in some suitable form and, then, to perform where needed a limiting procedure on the degrees of freedom corresponding to the higher order (linear, quadratic, etc.) basis functions after each sub-step of the Runge–Kutta procedure.

Let $\Delta t > 0$ denote a time step, and let $t^n = n\Delta t$, $n = 0, 1, \ldots$ Let $\mathbf{y}^n = \mathbf{y}(t^n)$. Given $\mathbf{y}^{n-1}$, the explicit Runge–Kutta scheme for solving (60) used in the RKΛΠP method is formulated as follows:

$$\begin{aligned} &\mathbf{y}^{(0)} = \mathbf{y}^{n-1}, \\ &\mathbf{y}^{(i)} = \sum_{l=0}^{i-1} \left[\alpha_{il}\mathbf{y}^{(l)} + \beta_{il}\Delta t \mathbf{L}_h(\mathbf{y}^{(l)}, t^{n-1} + \delta_l \Delta t)\right], \quad i = 1, \ldots, s, \\ &\mathbf{y}^n = \mathbf{y}^{(s)}. \end{aligned} \tag{61}$$

We have considered second- and third-order schemes. In the second-order scheme ($s = 2$), the coefficients are

$$\alpha_{10} = \beta_{10} = 1, \quad \alpha_{20} = \alpha_{21} = \beta_{21} = \frac{1}{2}, \quad \beta_{20} = 0, \quad \delta_0 = 0, \quad \delta_1 = 1. \tag{62}$$

Table 3
Advection-dominated advection–diffusion system $u = 1$, $D = 0.01$

k	Var.	Norm	$N = 40$	$N = 80$		$N = 160$	
			Error	Error	Order	Error	Order
0	s	$L^\infty(0,T;L^2)$	1.69e − 01	8.99e − 02	0.91	4.66e − 02	0.95
	z	$L^2(0,T;L^2)$	7.19e − 02	3.97e − 02	0.86	2.08e − 02	0.93
1	s	$L^\infty(0,T;L^2)$	1.68e − 03	4.32e − 04	1.96	1.13e − 04	1.93
	z	$L^2(0,T;L^2)$	1.93e − 02	9.83e − 03	0.97	4.97e − 03	0.98
2	s	$L^\infty(0,T;L^2)$	1.37e − 05	1.68e − 06	3.03	2.05e − 07	3.03
	z	$L^2(0,T;L^2)$	8.24e − 05	1.21e − 05	2.77	1.56e − 06	2.96

Table 4
Advection (purely hyperbolic) system $u = 1$, $D = 0$

k	Var.	Norm	$N = 40$	$N = 80$		$N = 160$	
			Error	Error	Order	Error	Order
0	s	$L^\infty(0,T;L^2)$	1.93e − 01	1.03e − 01	0.91	5.37e − 02	0.94
1	s	$L^\infty(0,T;L^2)$	1.61e − 03	4.00e − 04	2.01	9.99e − 05	2.00
2	s	$L^\infty(0,T;L^2)$	2.63e − 05	2.85e − 06	3.20	3.15e − 07	3.18

In the third-order scheme ($s = 3$), the coefficients are

$$\alpha_{10} = \beta_{10} = 1, \quad \alpha_{20} = \frac{3}{4}, \quad \alpha_{21} = \beta_{21} = \frac{1}{4}, \quad \beta_{20} = 0,$$
$$\alpha_{30} = \frac{1}{3}, \quad \beta_{30} = \alpha_{31} = \beta_{31} = 0, \quad \alpha_{32} = \beta_{32} = \frac{2}{3},$$
$$\delta_0 = 0, \quad \delta_1 = 1, \quad \delta_2 = \frac{1}{2}. \tag{63}$$

Next, we define the local projection operator $\Lambda\Pi$, which is the second important component of the RK$\Lambda\Pi$P methods. This operator is used to limit the higher order terms in the polynomial approximation, in order to prevent oscillations. We describe this limiting procedure in one-space-dimension. Descriptions of the procedure in multiple dimensions are given in [12,17].

We will expand functions $v \in W_h$ in terms of orthonormalized Legendre polynomials $l_k(x)$ on each subinterval B_j. These polynomials satisfy

$$\int_{B_j} l_q(x) l_p(x)\, \mathrm{d}x = \begin{cases} 1 & \text{if } q = p, \\ 0 & \text{otherwise.} \end{cases} \tag{64}$$

Consider the function

$$\tilde{m}(a_1, a_2, \ldots, a_n) = \begin{cases} a_1 & \text{if } |a_1| \leqslant M\Delta x^2, \\ m(a_1, a_2, \ldots, a_n) & \text{otherwise,} \end{cases} \tag{65}$$

where M is some positive number related to the second derivative of the true solution (for a detailed discussion of criteria for the choice of M see [14]), and m is the minmod function

$$m(a_1, a_2, \ldots, a_n) = \begin{cases} s \cdot \min |a_i| & \text{if } \operatorname{sign}(a_1) = \operatorname{sign}(a_2) = \cdots = \operatorname{sign}(a_n) = s, \\ 0 & \text{otherwise.} \end{cases} \tag{66}$$

Let $v \in W_h$, in the Legendre polynomial basis v can be expressed as follows:

$$v\,|_{B_j} = \sum_{r=0}^{k} v_j^{(r)} l_r(x). \tag{67}$$

Then, the local projection operator $\Lambda\Pi$ is defined by $v^* = \Lambda\Pi(v)$, where

$$v_j^{*(0)} = v_j^{(0)},$$
$$v_j^{*(1)} = \tilde{m}(v_j^{(1)}, v_{j+1}^{(0)} - v_j^{(0)}, v_j^{(0)} - v_{j-1}^{(0)}),$$
$$v_j^{*(r)} = \begin{cases} v_j^{(r)} & \text{if } v_j^{*(1)} = v_j^{(1)}, \\ 0 & \text{otherwise,} \end{cases} \quad r = 2, \ldots, k. \tag{68}$$

Fig. 1 illustrates the effect of the local projection operator on a piecewise linear function (we assume here $M = 0$).

The RK$\Lambda\Pi$P time-stepping method can be summarized as follows:

(i) Set $\mathbf{y}_0 = \mathbf{P}_h(\mathbf{y}(t_0))$, where $\mathbf{P}_h$ is the projection operator into W_h;

(ii) for $n = 1, 2, \ldots$ compute

$$\mathbf{y}^{(0)} = \mathbf{y}^{n-1},$$
$$\mathbf{y}^{(i)} = \Lambda\Pi\left(\sum_{l=0}^{i-1} \left[\alpha_{il} \mathbf{y}^{(l)} + \beta_{il} \Delta t \mathbf{L}_h(\mathbf{y}^{(l)}, t^{n-1} + \delta_l \Delta t) \right] \right), \quad i = 1, \ldots, s,$$
$$\mathbf{y}^n = \mathbf{y}^{(s)}. \tag{69}$$

For pure advection problems, it can be shown that the scheme above is total variation diminishing (TVD), provided the time-step satisfies certain CFL time-step restrictions. For stability, convergence and error estimates of the method (69) we refer to [13–15,17].

5. Numerical results for contaminant transport problems

In this section, we present some numerical results obtained using the LDG method applied to some problems of contaminant transport.

5.1. One-component contaminant transport problems

Consider the equation

$$c_t + \psi(c)_t + uc_x - Dc_{xx} = 0, \quad 0 < x < 1, \quad t > 0, \tag{70}$$

where $\psi(c) = (c)/(1 + c)$, $u = 1$, with the initial and boundary conditions

$$c(x, 0) = 0, \quad 0 < x < 1, \tag{71}$$
$$c(0, t) = 1, \quad t > 0, \tag{72}$$
$$c(1, t) = 0, \quad t > 0. \tag{73}$$

First, we show some examples illustrating the effect of the local projection operator on oscillatory behavior. The time-stepping scheme (69) of third-order is used. This problem has a discontinuous solution, as given in [30], and we obtain the results in Fig. 2 at time $T = 0.5$ for linear and quadratic approximating spaces. We see that the local projection operator removes the oscillatory behavior for both piecewise linear and piecewise quadratic approximating spaces.

Fig. 3 illustrates the solutions with and without physical diffusion. Here, we computed an approximate solution to the problem above at times $T \in \{0.2, 0.5, 0.8\}$ using the LDG method with piecewise constant approximating functions on 320 elements for $D = 0$ and $D = 0.01$. Since the piecewise constant approximations

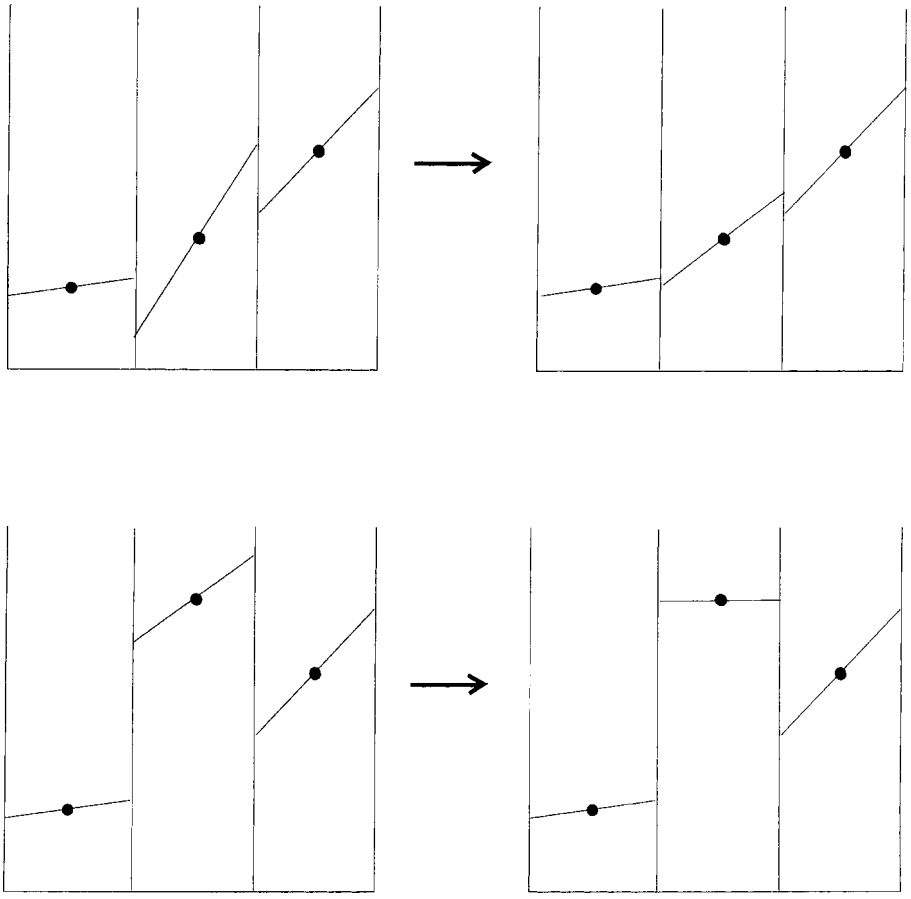

Fig. 1. Effect of the local projection operator on a piecewise linear function.

are not susceptible to oscillatons, the local projection procedure is not needed in these computations.

5.2. Two-component contaminant transport problems

More interesting and challenging problems arise in multi-component contaminant transport models. We repeated the above experiments for a two-component case. Consider the advection–diffusion system

$$\mathbf{c}_t + \Psi(\mathbf{c})_t + u\mathbf{c}_x - D\mathbf{c}_{xx} = 0, \quad 0 < x < 1, \ t > 0, \tag{74}$$

where $u = 1$, the isotherm function is

$$\Psi(\mathbf{c}) = \begin{pmatrix} \dfrac{c_1}{1 + c_1 + 10c_2} \\ \dfrac{10c_2}{1 + c_1 + 10c_2} \end{pmatrix}, \tag{75}$$

and the initial and boundary conditions are

$$\mathbf{c}(x,0) = \begin{pmatrix} 0 \\ 0 \end{pmatrix}, \quad 0 < x < 1, \tag{76}$$

$$\mathbf{c}(0,t) = \begin{pmatrix} 1 \\ 1 \end{pmatrix}, \quad t > 0, \tag{77}$$

$$\mathbf{c}(1,t) = \begin{pmatrix} 0 \\ 0 \end{pmatrix}, \quad t > 0. \tag{78}$$

First, we examine the effect of the local projection operator on the numerical solutions for the case $D = 0$. From the results in Fig. 4, we see that the local projection operator provides us with an effective post-processing algorithm, capable of suppressing oscillatory behavior.

In Fig. 5, we show approximate solutions to the problems (74)–(78) at times $T \in \{0.2, 0.5, 0.8\}$ using the LDG method with piecewise constant approximating functions on 320 elements for $D = 0$ and $D = 0.01$. For $D = 0$, we obtain a moving shock wave and the numerical solution agrees very well with the theoretical results presented in [30].

The next test further illustrates the impact of the diffusion term on the shape of the wave. Here, we compute an approximate solution to the system (74) with the initial and boundary conditions (76)–(78) and the isotherm function (75) at time $T = 0.5$ for $D \in \{0, 0.01, 0.05\}$: see Fig. 6.

In the following numerical experiments, we compare results of computations on the same test problem by the LDG method using approximating spaces of different order. First, we test the hyperbolic system obtained from 74 by setting $D = 0$ with the initial and boundary conditions (76)–(78) and isotherm (75) at time $T = 0.5$, see

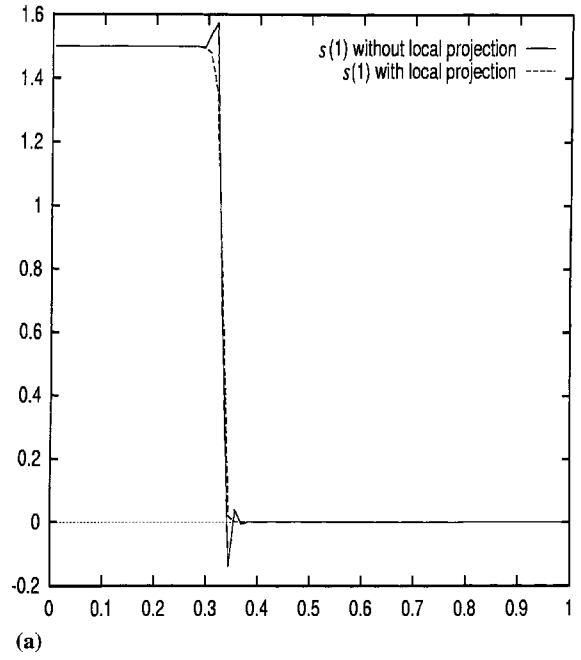

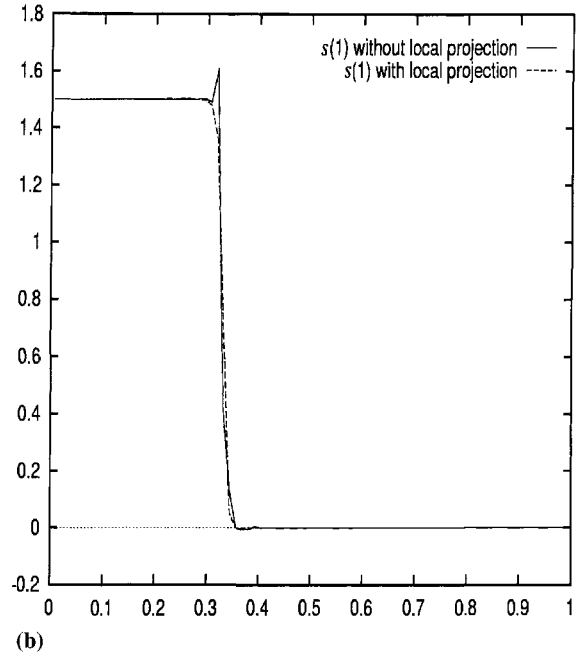

Fig. 2. Influence of the local projection operator on oscillatory behavior (scalar equation case): (a) piecewise linear approximating functions, 80 elements; (b) piecewise quadratic approximating functions, 80 elements.

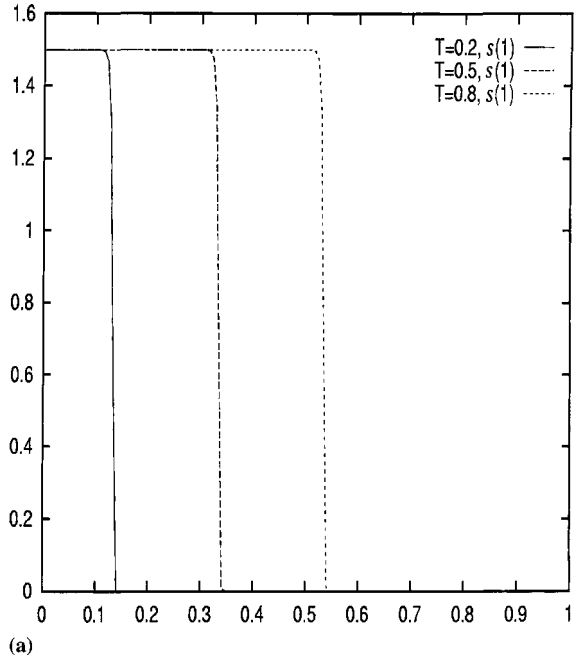

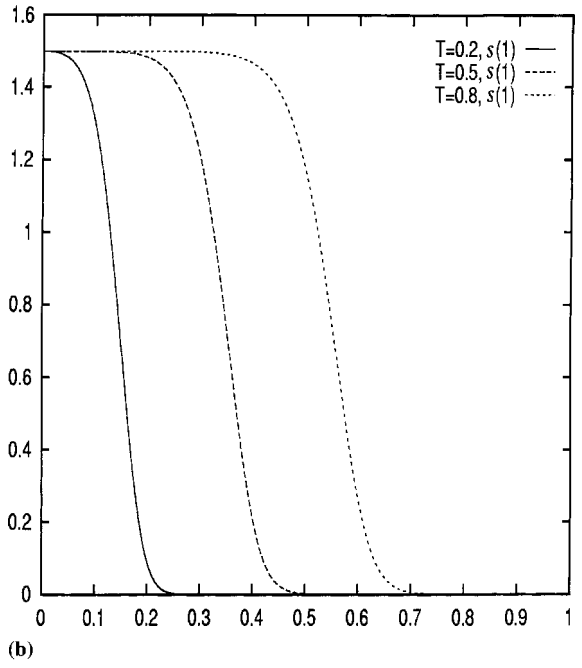

Fig. 3. Effect of the diffusion term on the solution (scalar equation case): (a) advection equation, $D = 0$; (b) advection-dominated advection–diffusion equation, $D = 0.01$.

Fig. 7. Piecewise constant, linear and quadratic approximations were used. Use of piecewise linear approximating polynomials required the local projection procedure to be carried out after each sub-time-step. However, as expected, the piecewise linear approximation gives us clearly much sharper resolution of the shock wave than the piecewise constant approximation. The piecewise quadratic solution gives very similar results to the piecewise linear solution for this level of resolution. We next conduct a similar test for the parabolic system (74) with $D = 0.01$, the same initial and boundary conditions, and the same isotherm as in the previous example. Constants, linear and quadratic approximations are used. In Fig. 8, we see that all three approximate solutions lie very close together. In this example, we used different meshes and different

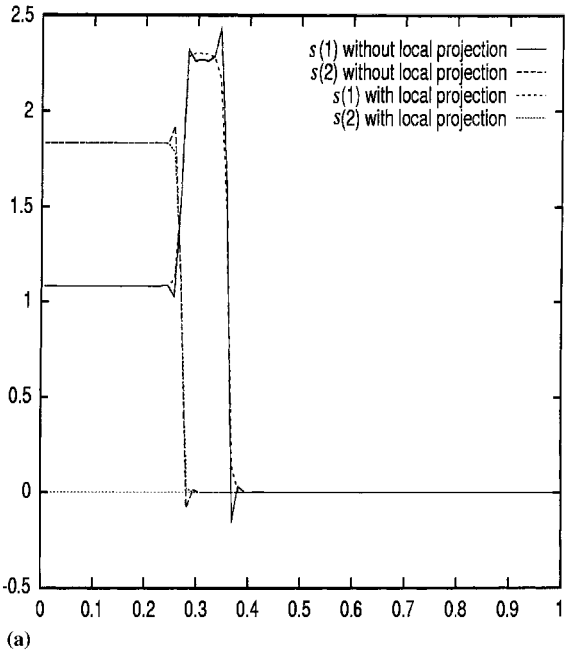

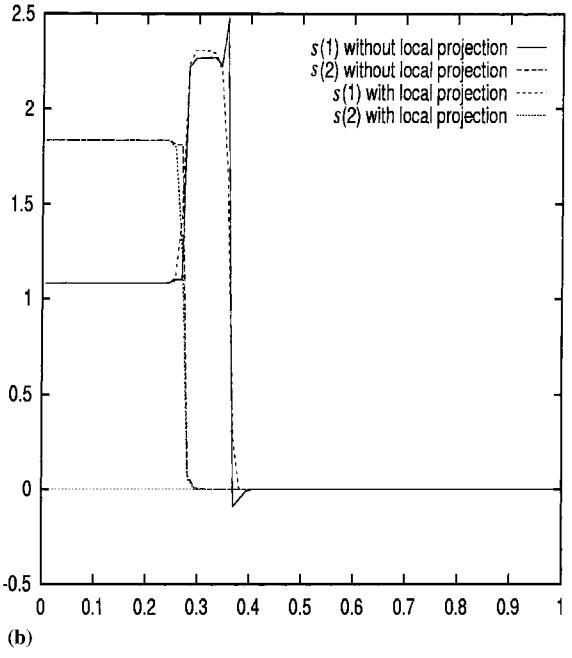

Fig. 4. Influence of the local projection operator on oscillatory behavior (system case): (a) piecewise linear approximating functions, 80 elements; (b) piecewise quadratic approximating functions, 80 elements.

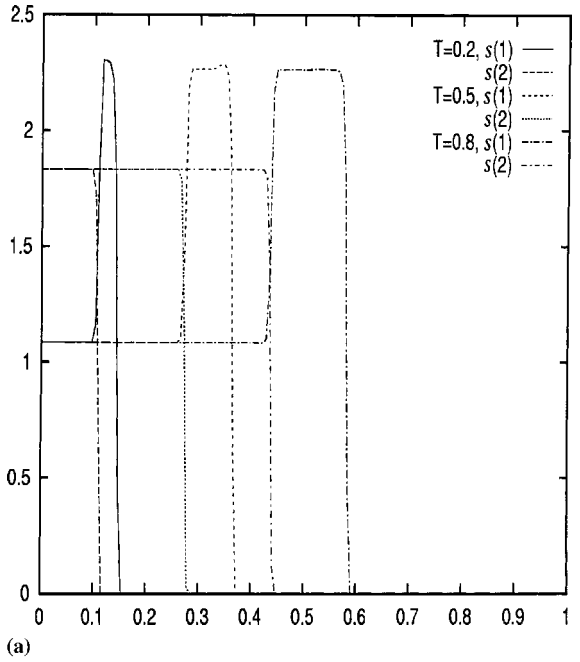

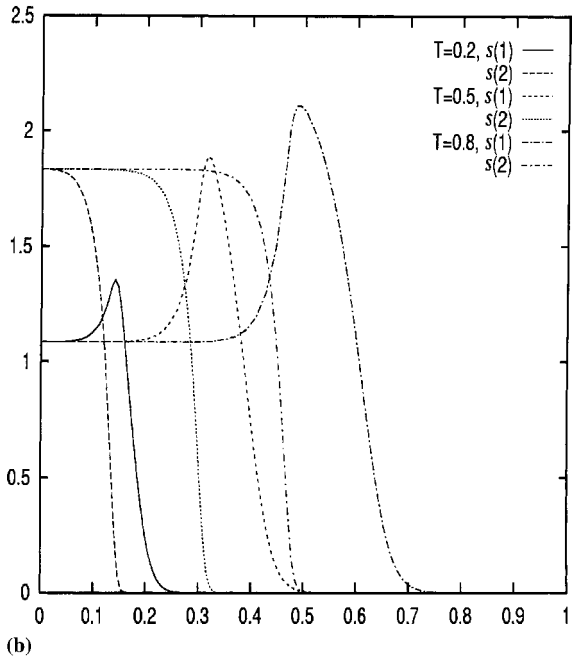

Fig. 5. Effect of the diffusion term on the solution (system case): (a) advection system, $D = 0$; (b) advection-dominated advection–diffusion system, $D = 0.01$.

time-stepping schemes for the different approximations. For constants, we used forward Euler time-stepping, thus the degrees of freedom computed per time step for this solution is 640. For linears, we used a second-order Runge–Kutta procedure, thus the degrees of freedom computed per time step are also $160 * 2 * 2 = 640$. Similarly, for quadratics a third-order Runge–Kutta procedure was used, requiring the computation of $80 * 3 * 3 = 720$ degrees of freedom per time step. In this case, the use of the coarser meshes for linears and quadratics allows for the use of larger time steps, due to the CFL constraint. Compared to the constant case, we were able to use a time step four times larger to compute the linear solution, and eight times larger to compute the quadratic solution. This example points out one of the benefits of using higher order polyno-

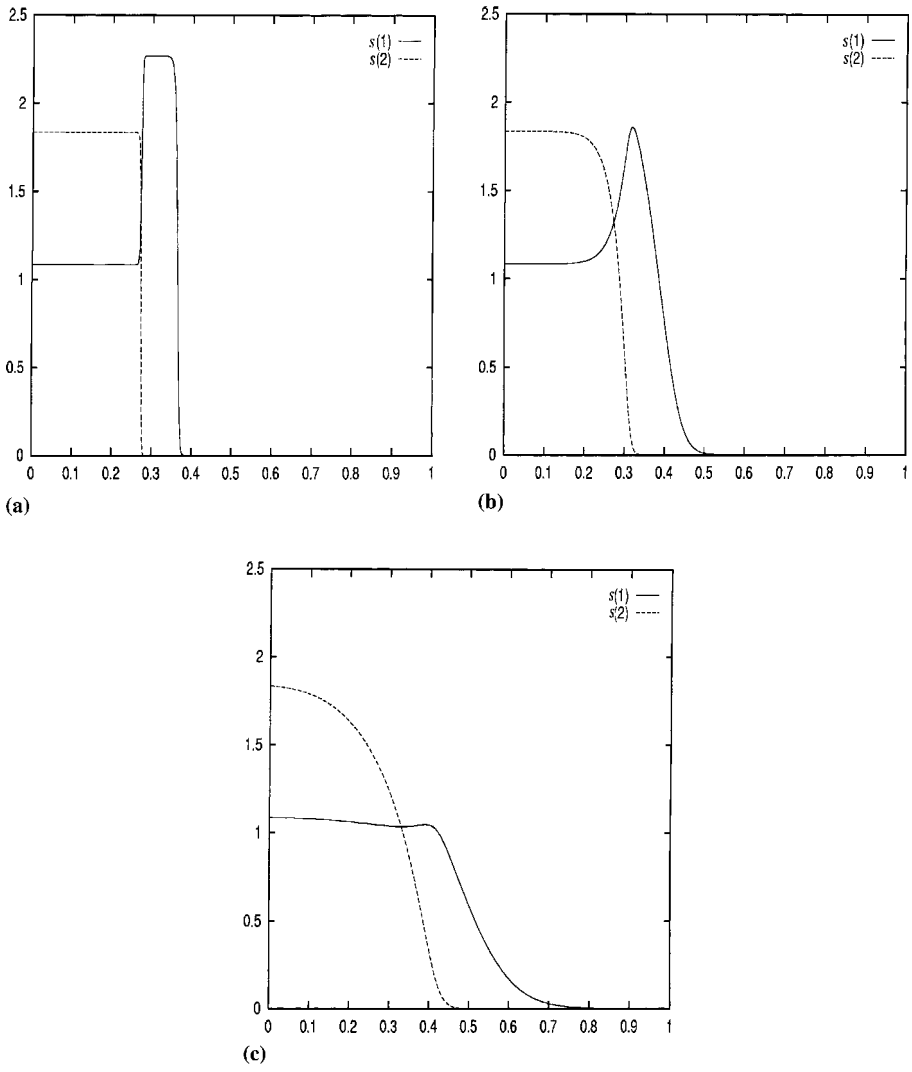

Fig. 6. Impact of the diffusion term on the shape of the wave: (a) advection system, $D = 0$; (b) advection-dominated advection–diffusion system, $D = 0.01$; (c) advection-dominated advection–diffusion system, $D = 0.05$.

mials, at least for problems with a sufficient amount of diffusion.

5.3. Some preliminary two-dimensional results

We are currently in the process of developing a two-dimensional transport code using the LDG method with adaptive triangular grids. Here, we present a preliminary result on a standard advection problem. A more thorough study of multi-dimensional problems will be considered in a future paper.

We consider the "rotating hill" problem

$$c_t - (2\pi yc)_x + (2\pi xc)_y = 0 \tag{79}$$

with analytical solution

$$c(x,y,t) = 5\exp(-20(x\cos(2\pi t) + y\sin(2\pi t) - 0.6)^2 + (-x\sin(2\pi t) + y\cos(2\pi t))^2.) \tag{80}$$

We began with an initial mesh of 76 elements, and refined this mesh three times, where each refinement was obtained by dividing each triangle into four smaller triangles. We refer to the coarsest mesh as mesh 1, and successive meshes as mesh 2, 3 and 4. In Fig. 9, we compare the linear solution on mesh 4, the quadratic solution on mesh 3, the cubic solution on mesh 2 and the quartic solution on mesh 1. All solutions are at $t = 1$, which represents one full rotation of the hill. Here, we have taken a small time step and used the same temporal integration scheme for each method. As indicated in the figure, the solutions are very similar. The degrees of freedom/time step for each case are 14,592 for the linear solution, 7296 for the quadratic solution, 3040 for the cubic solution and 1140 for the quartic solution. The rate of convergence for each case is illustrated in Table 5. Here, we have computed the rate of convergence by comparing the ratio of errors on successive meshes. That is,

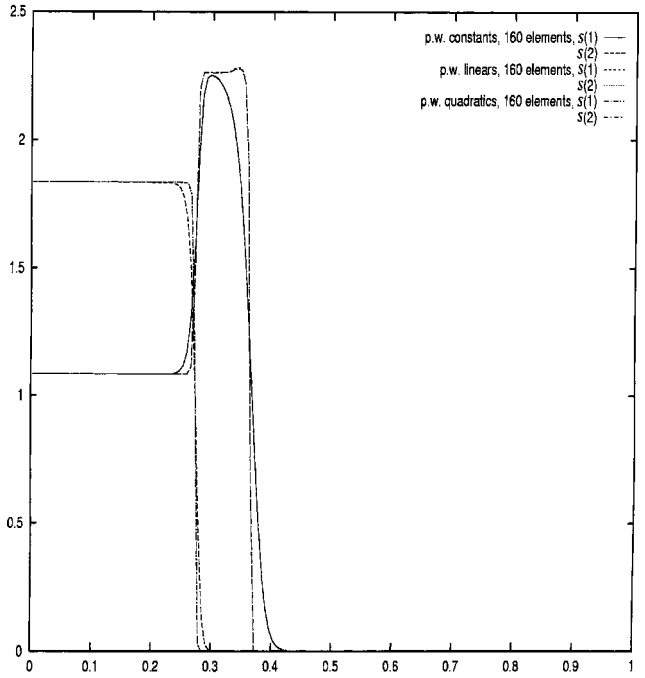

Fig. 7. Comparison of solutions obtained using different approximating spaces (hyperbolic system).

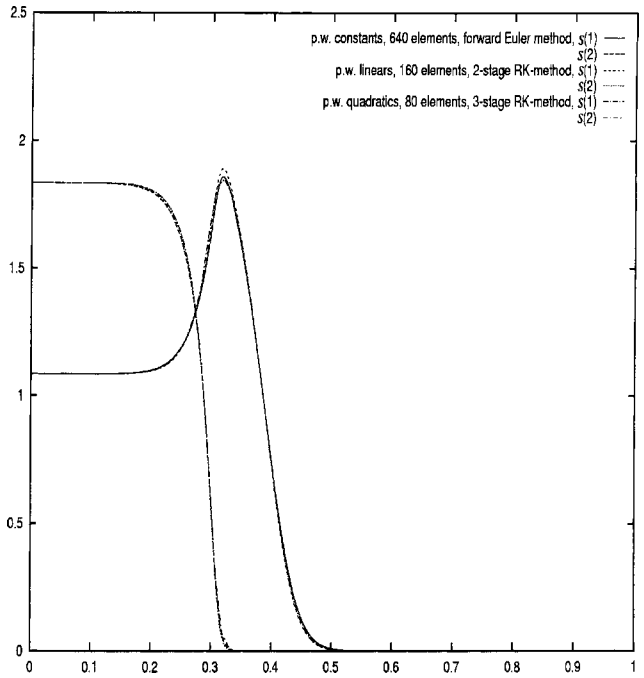

Fig. 8. Comparison of solutions, obtained using different approximating spaces (parabolic system).

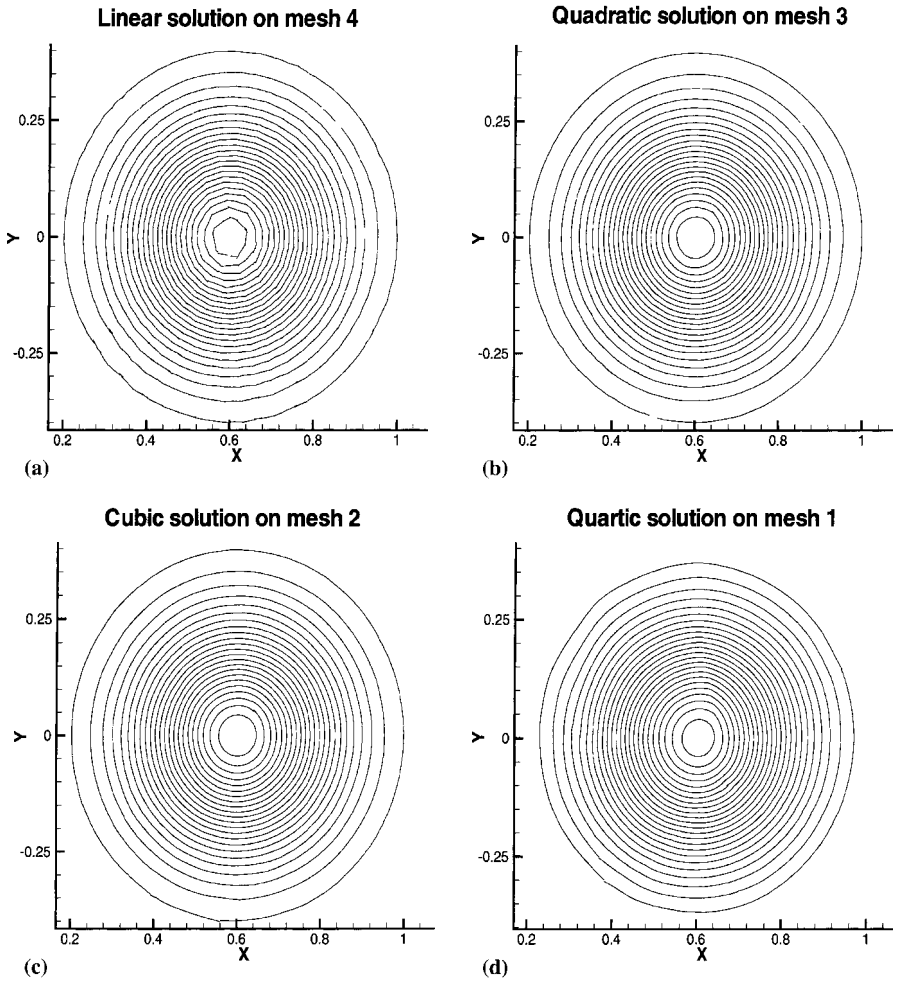

Fig. 9. Rotating hill problem. Comparison of different degree polynomials on different meshes.

Table 5
Rotating hill problem

k	Rate_1	Rate_2	Rate_3
1	1.2	2.27	2.87
2	2.87	3.58	3.17
3	4.57	4.78	4.21
4	5.48	4.90	4.76

$$\text{Rate}_i = \log\left(\frac{E_{i+1}}{E_i}\right) \Big/ \log(0.5), \tag{81}$$

where E_i is the L^2 error on mesh i. Note that for polynomial degrees 2–4, the rate of convergence seems to be approaching $k+1$, which agrees with our one-dimensional results. The rate of convergence in the linear case appears to be better than second-order, but this is probably because we are not into the asymptotic range yet, as the errors are still somewhat oscillatory.

We conclude this section with an examination of "price vs performance" for the problem above. In Fig. 10, we have plotted CPU/time step vs error on a log–log scale for the four different meshes described above, and for polynomials of degree up to six. Each line corresponds to a different mesh, with the symbols on each line representing the error for the six different approximating spaces. From the figure, we observe that in general the higher degree polynomials give a more accurate solution with smaller CPU time. Thus, the use of higher order approximations, at least in smooth parts of the solution, is worth further investigation.

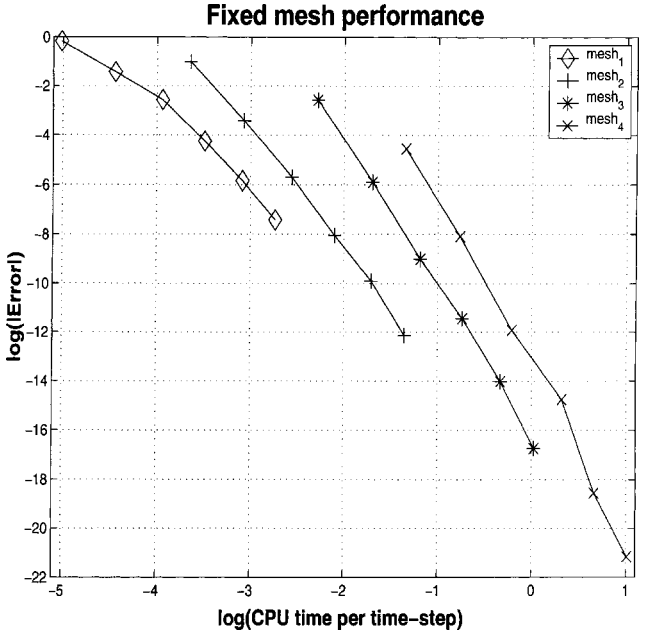

Fig. 10. Comparison of CPU/time step vs L^2 error for four successively refined meshes and polynomials of degree 1–6.

6. Concluding remarks

In this paper, we have described a new discontinuous finite element method for contaminant transport equations. This method is built upon the discontinuous Galerkin method for pure advection equations, which has been shown in a series of papers to perform well on both linear and non-linear problems [2,12–16]. This scheme is applicable to non-linear systems of equations and easily extends to multi-dimensions. The scheme performs well on solutions with sharp fronts as well as for smooth problems. It also allows for the use of higher degree polynomials while still preserving the stability of the solution.

We are currently in the process of implementing the method for multi-dimensional problems, with adaptive grid refinement/derefinement. The results of these investigations will be the subject of future work.

References

[1] Arbogast T, Bryant S, Dawson C, Saaf F, Wang C. Computational methods for multiphase flow and reactive transport problems arising in subsurface contaminant remediation. J Comp Appl Math 1996;74:19–32.
[2] Akins H, Shu C-W. Quadrature-free implementation of discontinuous Galerkin methods for hyperbolic equations. AIAA J 1998;36:775–82.
[3] Barrett JW, Knabner P. Finite element approximation of transport of reactive solutes in porous media part 1. Error estimates for equilibrium adsorption processes. SIAM J Numer Anal 1997;34:201–27.
[4] Barret JW, Knabner P. Finite element approximation of transport of reactive solutes in porous media part 2. Error estimates for equilibrium adsorption processes. SIAM J Numer Anal 1997;34:455–79.
[5] Brenner S, Scott LR. The mathematical theory of finite element methods. New York: Springer; 1994.
[6] Butcher JC. The numerical analysis of ordinary differential equations. New York: Wiley; 1987.
[7] Castillo P, Cockburn B, Perugia I, Schotzau D. An a priori error analysis of the local discontinuous Galerkin method for elliptic problems. To appear.
[8] Castillo P, Cockburn B, Schotzau D, Schwab C. Optimal a priori error estimates for the *hp*-version of the local discontinuous Galerkin method for convection–diffusion problems. Math Comp. To appear.
[9] Chavent G, Jaffré J. Mathematical models and finite elements for reservoir simulation. Amsterdam: North-Holland; 1986.
[10] Chen Q, Zhao D, Tabios IGQ, Shen HW. 2D coupled water quality model for industrial effluent transport. In: Proceedings of the 1998 International Water Resource Engineering Conference, vol. 2. ASCE, 1998. p. 1637–42.
[11] Cockburn B, Dawson C. Some extensions of the local discontinuous Galerkin method for convection–diffusion equations in multidimensions. Technical Report 99-27. Texas Institute for Computational and Applied Mathematics. The University of Texas at Austin. August 1999.
[12] Cockburn B, Hou S, Shu CW. TVB Runge–Kutta local projection discontinuous Galerkin finite element method for conservation laws IV: the multidimensional case. Math Comp 1990;54:545–81.

[13] Cockburn B, Lin SY, Shu CW. TVB Runge–Kutta local projection discontinuous Galerkin finite element method for conservations laws III: one dimensional systems. J Comput Phys 1989;84:90–113.
[14] Cockburn B, Shu CW. TVB Runge–Kutta local projection discontinuous Galerkin finite element method for scalar conservations laws II: general framework. Math Comp 1989;52:411–35.
[15] Cockburn B, Shu CW. The Runge–Kutta local projection P^1-discontinuous Galerkin method for scalar conversations laws. M^2AN 1991;25:337–61.
[16] Cockburn B, Shu CW. The local discontinuous Galerkin method for time dependent convection–diffusion systems. SIAM J Numer Anal 1998;35:2440–463.
[17] Cockburn B, Shu CW. TVB Runge–Kutta discontinuous Galerkin finite element method for conservations laws V: multidimensional systems. J Comput Phys 1998;141: 199–224.
[18] Dawson C, Aizinger V. Upwind mixed methods for transport equations. Comput Geosci 1999;3:93–110.
[19] Dawson C, Proft J. The local discontinuous Galerkin method with penalties for parabolic problems. To appear.
[20] Dawson C, van Duijn CJ, Grundy RE. Large-time asymptotics in contaminant transport in porous media. SIAM J Appl Math 1996;56:965–93.
[21] Dawson C, van Duijn CJ, Wheeler MF. Characteristic-Galerkin methods for contaminant transport with non-equilibrium adsorption kinetics. SIAM J Numer Anal 1994;31:982–99.
[22] Dawson CN. Godunov-mixed methods for advective flow problems in one space dimension. SIAM J Numer Anal 1991;28:1282–309.
[23] Dawson CN. Godunov-mixed methods for advection–diffusion equations in multidimensions. SIAM J Numer Anal 1993;30: 1315–32.
[24] Diersch H-JG. Shock-capturing finite-element technique for unsaturated–saturated flow and transport problems. In: Proceedings of the 12th International Conference on Computational Methods in Water Resources, vol. 1. Computational Mechanics Publications, 1998. p. 207–14.
[25] Dortch MS, Ruiz C, Geral T, Hall RW. Three-dimensional contaminant transport/fate model. In: Proceedings of the Fifth International Conference on Estuarine and Coastal Modeling. ASCE, 1997. p. 75–89.
[26] Gallo C, Manzini G. 2D numerical modeling of bioremediation in heterogeneous saturated soils. Transp Porous Media 1998;31:67–88.
[27] Gallo C, Manzini G. Mixed finite element/volume approach for solving biodegradation transport in groundwater. Int J Numer Meth Fluids 1998;26:533–56.
[28] Grundy RE, van Duijn CJ, Dawson CN. Asymptotic profiles with finite mass in one-dimensional contaminant transport through porous media: the fast reaction case. Quart J Mech Appl Math 1994;47:69–106.
[29] LeVeque RJ. Numerical methods for conservation laws. Basel: Birkhauser; 1992.
[30] Rhee HK, Aris R, Amundson NR. First-order partial differential equations. Englewood Cliffs, NJ: Prentice-Hall; 1989.
[31] Sankaranarayanan S, Shankar NJ, Cheong HF. Three-dimensional finite difference model for transport of conservative pollutants. Ocean Eng 1998;25:425–42.
[32] Siegel P, Mose R, Ackerer P, Jaffre J. Solution of the advection–diffusion equation using a combination of discontinuous and mixed finite elements. Int J Numer Meth Fluids 1997;24:595–613.
[33] van Duijn CJ, Grundy RE, Dawson CN. Large-time profiles in reactive solute transport media. Transp Porous Media 1997;27:57–84.
[34] van Duijn CJ, Knabner P. Solute transport in porous media with equilibrium and non-equilibrium multiple-site adsorption: travelling waves. J Reine Angewandte Math 1991;415:1–49.
[35] Weber JWJ, McGinley PM, Katz LE. Sorption phenomena in subsurface systems: concepts, models and effects on contaminant fate and transport. Water Res 1991;25:499–528.
[36] Wang H, Falconer RA. Simulating disinfection processes in chlorine contact tanks using various turbulence models and high-order accurate difference schemes. Water Res 1998;32:1529–43.
[37] Yu M, Dougherty DE. FCT model of contaminant transport on unstructured meshes. In: Proceedings of the 12th International Conference on Computational Methods in Water Resources, vol. 1. Computational Mechanics Publications, 1998. p. 199–206.
[38] Zhao D, Lai JS, Hsieh WS. Two-dimensional contaminant transport model with high resolution upwind scheme. In: Proceedings of the 1994 ASCE National Conference on Hydraulic Engineering. ASCE, 1994. p. 135–39.